Generalized transfer function: A simple model applied to active single-mode microring resonators

Yann G. Boucher, Patrice Feron

Generalized transfer function: A simple model applied to active single-mode microring resonators

Y.G. Boucher [a,b,c,*], P. Féron [b,c]

[a] RESO Laboratory (EA 3380), ENIB, CS 73862, F-29238 Brest Cedex 3, France
[b] ENSSAT–FOTON (CNRS–UMR 6082), Université de Rennes-1, 6 rue de Kerampont, BP 80518, 22305 Lannion Cedex, France
[c] Université européenne de Bretagne, France

The spectral properties of an active single-mode microring resonator are investigated in the frame of the generalized transfer function (GTF) approach, as derived from extended scattering and/or transfer matrix formalism. Spontaneous emission, looked upon as the driving source of the radiation, is described in a semi-classical way in the spectral domain. The internal and emitted fields are filtered into the resonance modes of the whole structure. The generalized transfer function expresses the spectral density of internal saturating intensity and includes all essential mechanisms at work in a laser oscillator: gain, losses and sources. The active zone is saturated through amplified spontaneous emission (ASE), integrated over its whole spectral range. Continuously valid across threshold, the method enables one to derive in a simple way the main steady-state properties of the laser oscillation, with the pumping rate as the only external parameter.

1. Introduction

In the past few years, optical open resonators based on total internal reflection (TIR) such as microspheres, microdisks or microrings have been subject to numerous studies [1,2]. The unique combination of strong temporal and spatial confinement of light makes these systems particularly attractive, not only for fundamental research [3,4] but also as new building blocks for fiber optics and photonic applications [5]. For instance, a review of photonic structures based on highly integrated passive coupled microrings can be found in Refs. [6,7]. Naturally enough, active structures have also been heavily investigated. Since the observation of the first continuous-wave (CW) laser oscillation in a large solid-state Nd:YAG sphere [8], laser action has been demonstrated in many different rare-earth-doped glass spheres [9,10], as well as semiconductor microdisks [11,12] or microrings [13].

As soon as optical gain is involved, spontaneous emission is known to play quite important a role: far from being a mere noise to be avoided, it acts as the very driving source of the electromagnetic field. In that respect, the laser behavior of single-mode Fabry–Perot (FP) resonators is well depicted in the spectral domain by the semi-classical generalized transfer function (GTF) [14,15]. The GTF expresses the spectral density of the internal field, where the gain, the source and the refractive index of the active zone are uniformly saturated through amplified spontaneous emission (ASE), longitudinally averaged and integrated over its whole spectral range. Assuming the total saturating intensity as the only internal parameter, a self-consistent calculation enables one to derive the total power as well as the lineshape of the emitted radiation, as functions of the pumping level.

In its turn, the GTF of a one-dimensional active cavity can be conveniently established in the frame of the extended (3×3) transfer matrix formalism. This elegant way of dealing with internal sources had been originally proposed by Weber and Wang [16,17] for investigating active distributed feedback (DFB) devices, and further developed by one of us well into the laser regime. An analytical expression for the GTF is easily derived in terms of structural parameters, leading to a self-consistent calculation of all parameters as soon as the saturation of the active medium is correctly taken into account [18,19].

* Corresponding author. Address: RESO Laboratory (EA 3380), ENIB, CS 73862, F-29238 Brest Cedex 3, France. Tel.: +33 2 98 05 66 66; fax: +33 2 98 05 66 89.
E-mail address: boucher@enib.fr (Y.G. Boucher).

Considering the enormous potential of such a formalism for the active FP cavity, or more generally for any kind of one-dimensional resonator, including multisection structures, it seemed natural to investigate its adaptation to active resonators with other geometries. The transposition is not straightforward, though: from a physical point of view, a ring resonator differs from a FP cavity by its traveling wave behaviour (quite different from the standing wave pattern). Above all, from a technical point of view, because of its loop topology, a ring cannot be decomposed into cascadable matrices. Therefore, a specific approach is needed: in that respect, "extended scattering parameters" (as introduced hereafter) appear as a useful tool for expressing the relationships between the relevant waves that travel inside the ring resonator, with the spontaneous contributions included.

The present work is devoted to the specific case of an active single-mode microring resonator, coupled to a passive straight waveguide that acts as input/output ports. We would like to emphasise that the main appeal of our model lies with its astounding simplicity. Besides, it can be used to describe, indifferently, either a selective amplifier (below threshold) or a laser oscillator (above threshold). We show how the spontaneous field generated by an active zone is coupled into the resonance modes of the structure, that eventually determine the spectral lineshape. We give simple and generic expressions for the spontaneous contributions in terms of equivalent fields that couple into the mode. Since we are mainly concerned with structural properties, no restriction is made a priori regarding the materials themselves. For the sake of simplicity, thermal effects are not considered until the very end: an external control of temperature is therefore implicitly assumed.

Our paper is organized as follows. In Section 2, we recall the main features of the "classical" transfer function of the device. The spectral density of emitted radiation is derived in the frame of extended transfer and/or scattering matrix formalisms including sources. The spectral density of internal saturating field, or generalized transfer function, is exposed in Section 3; the effect of material dispersion is illustrated on a concrete example, since we present a complete self-consistent determination, in normalized parameters, of the threshold-crossing in a ring filled with an homogeneously broadened atomic gain medium. We derive analytical expressions that remain continuously valid across threshold. Possible further developments and perspectives, such as thermal effects, extended cavity schemes, a structure made of a ring connected to two parallel straight waveguides or the case of optical seeding, are briefly outlined, along with conclusions, in Section 4.

2. Transfer function and extended matrix formalism

2.1. Classical transfer function

Consider a ring resonator (of propagation constant β_R and perimeter L_R) coupled to a straight waveguide (of propagation constant β_S and length L_S), as depicted in Fig. 1a. Both waveguides are supposed transversally single-mode, and we neglect polarization effects, so that the waves are purely scalar. Time dependence is taken as $\exp(+i\omega t)$.

Following Yariv [20], we use simple analytical formulas based on structural parameters. One key element is the linear coupler between the rectilinear waveguide and the ring, seen as a four-port network (Fig. 1b). It is completely determined by three parameters t_c, t'_c, and k_c. Let us call $\eta^2 = (t_c t'_c - k_c^2)$; $\gamma = \exp(g_R L_R/2)$ and $\exp(-i\mathrm{Re}[\beta_R]L_R)$ are the amplitude and phase change over the ring, respectively, with g_R its modal gain. This expression remains valid whatever the gain or loss level: $\gamma = 1$ in a transparent medium, $\gamma > 1$ in an amplifier, $\gamma < 1$ in case of absorption. Internal ports 3 and 4 are connected through:

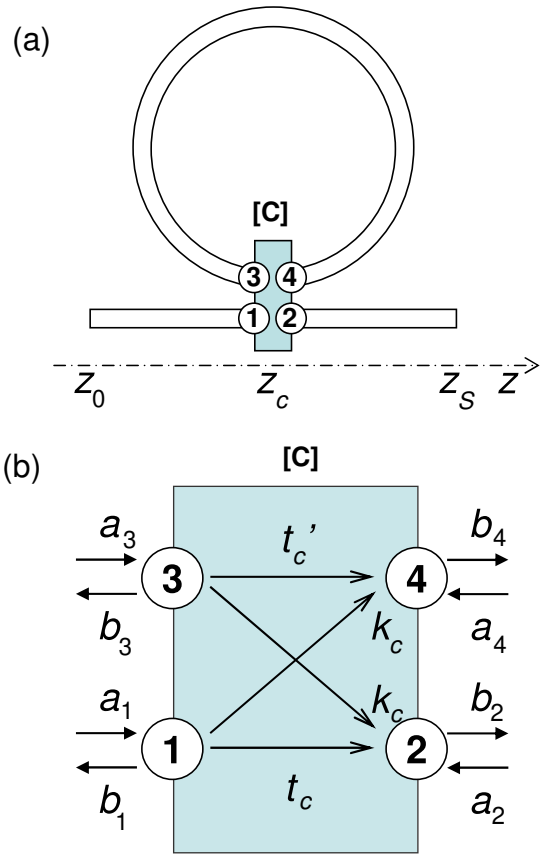

Fig. 1. Single-mode ring waveguide connected to a single-mode straight waveguide. (a) Geometrical configuration. (b) Notations for the coupler seen as a four-port network.

$$a_3 = b_4\,\gamma\,\exp\left(-i\,\mathrm{Re}[\beta_R]\,L_R\right), \tag{1a}$$

$$a_4 = b_3\,\gamma\,\exp\left(-i\,\mathrm{Re}[\beta_R]\,L_R\right). \tag{1b}$$

Between remaining ports 1 and 2, the complex transmittance t_R reads:

$$t_R = \frac{t_c - \eta^2\,\gamma\,\exp\left(-i\,\mathrm{Re}[\beta_R]\,L_R\right)}{1 - t'_c\,\gamma\,\exp\left(-i\,\mathrm{Re}[\beta_R]\,L_R\right)}. \tag{2}$$

Without loss of generality, we can shift the reference planes in order for the coupler to be completely localized at abscissa z_c. In that case, it is legitimate to assume that $t'_c = t_c^* = \eta\,\tau_0\,\exp(-i\,\varphi_c)$, where τ_0 denotes the value of $|t_c|$ in the lossless coupler, whereas η^2 becomes a real number at most equal to unity, representative of the coupler losses. With $\Phi = \mathrm{Re}[\beta_R]\,L_R + \varphi_c$ the overall phase change over a round-trip, the denominator $D_R = [1 - \tau_0\,\eta\,\gamma\,\exp(-i\,\Phi)]$ presents the typical signature of a spectrally selective resonance. The "classical" transfer function in intensity $T_R = |t_R|^2$ can be expressed as

$$T_R(\Phi) = \eta^2\left\{1 + \frac{T_0 - 1}{1 + m_R\,\sin^2\left(\Phi/2\right)}\right\}, \tag{3a}$$

$$T_0 = \left(\frac{\tau_0 - \eta\,\gamma}{1 - \tau_0\,\eta\,\gamma}\right)^2, \tag{3b}$$

$$m_R = \frac{4\,\tau_0\,\eta\,\gamma}{\left(1 - \tau_0\,\eta\,\gamma\right)^2}. \tag{3c}$$

The whole system is thus completely determined by four independent parameters only: $(\eta, \tau_0, \gamma, \Phi)$, with $(\eta^2\,T_0)$ the transmission at resonance and m_R a factor of spectral selectivity.

In absence of net losses or gain, the ring resonator is purely dephasing ($\eta\gamma = 1 \Rightarrow \forall\Phi, T_R = 1$), and its phase is a non-linear function of Φ.

We draw in Fig. 2 the normalized transfer function $T_R(\Phi)/\eta^2$ for a given value of coupling τ_0, and different values of $\eta\gamma$, which represents the net amplitude change over a round-trip. For values of $\eta\gamma$ smaller than unity, the ring exhibits losses, especially important at resonance ($\Phi \equiv 0\,[2\pi]$) where T_R reaches its *minimum* ($T_0 < 1$); structural transparency is obtained for $\eta\gamma = 1$ and actual amplification for $\eta\gamma > 1$.

The resonance width itself is conditioned by the selectivity factor m_R, that is by $\tau_0\eta\gamma$ (Eq. (3)). As soon as m_R is much greater than unity, $1/|D_R|^2$ is well approximated by a Lorentzian lineshape: writing the phase as $\Phi = 2q\pi + \delta\Phi$ around a resonance (where q is an integer), we get:

$$\frac{1}{|D_R|^2} \approx \left\{ \frac{1/(\tau_0\eta\gamma)}{\delta\Phi^2 + (4/m_R)} \right\} \propto \frac{\Delta_R^2}{\delta\Phi^2 + \Delta_R^2}, \tag{4a}$$

$$\Delta_R = \frac{2}{\sqrt{m_R}} = \frac{(1-\tau_0\eta\gamma)}{\sqrt{\tau_0\eta\gamma}}. \tag{4b}$$

Since phase Φ depends almost linearly on angular frequency ω, the spectral transfer function $T_R(\omega)$ exhibits also a Lorentzian lineshape of half-width at half-maximum Γ_R (HWHM), upsurging from a constant plateau. In spectral terms, $\Gamma_R = \Delta_R(c/n_g L_R)$, where $n_g = n_{\text{eff}} + \omega(\partial n_{\text{eff}}/\partial\omega)$ is the group index, and $c/(n_g L_R)$ the free spectral range (FSR) of the ring resonator. Around a resonance frequency ω_0, the quality factor of the cavity is defined as $Q = (\omega_0/\Gamma_R)$.

In the amplification regime, the higher $\eta\gamma$, the higher the *maximum* transmission ($T_0 > 1$), the sharper the resonance. This holds true up to the oscillation: the classical *threshold* condition is reached for $\gamma = \gamma_{\text{th}} = 1/(\eta\tau_0)$. Mathematically, the linewidth should tend towards zero and T_0 towards the infinite at threshold; but this un-physical divergence does not actually occur, because of saturation mechanisms that will be commented upon below.

The main effect of losses inside the coupler is twofold, as illustrated in Fig. 3: (i) the transmission is affected ($\eta^2 T_0$ at resonance, η^2 off-resonance); (ii) the line-width is broadened. The first point proves especially interesting since a fitting value of η^2 can be adjusted experimentally on an actual device, by measuring the off-resonance transmission.

The transfer function, and especially the resonance expressed by denominator D_R, plays an important role in determining the spectral properties of the fields emitted by an active ring resonator with embedded sources.

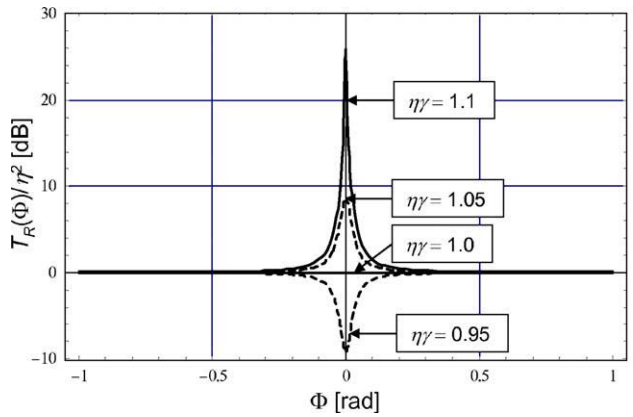

Fig. 2. Classical transfer function of the micro-ring. Normalized transmission $T_R(\Phi)/\eta^2$ with $\tau_0 = 0.9$, for $\eta\gamma = 0.95$ (absorption), 1 (transparency), 1.05 and 1.1 (amplification): The higher the net gain, the sharper the resonance.

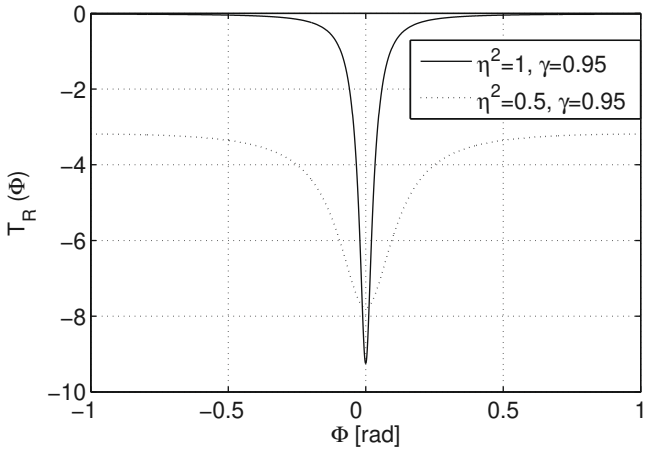

Fig. 3. Effects of coupling losses on the classical transfer function of an otherwise lossy ring: $\tau_0 = 0.9, \gamma = 0.95$ for $\eta^2 = 1$ (lossless coupler, straight line) and $\eta^2 = 0.5$ (-3 dB coupler, dashed line). Far from resonance, the transmission reaches asymptotically its highest possible value η^2; its absolute minimum at resonance is $\eta^2\ T_0$.

2.2. Extended matrix formulations

When internal sources are taken into account, the relationship between input and output waves is no longer linear (as in Eq. (1)), because of the intrinsic contribution of the active zone. In order to take the latter into account, we write:

$$a_3 = b_4\,\gamma\,\exp(-i\,\text{Re}[\beta_R]\,L_R) + (u^+), \tag{5a}$$

$$a_4 = b_3\,\gamma\,\exp(-i\,\text{Re}[\beta_R]\,L_R) + (u^-), \tag{5b}$$

where (u^+) and (u^-) represent the equivalent fields of spontaneous emission that couple into the ring mode at both "ends" of the active zone [21]; the sign $(+/-)$ is relative to the direction of propagation along the z-axis at the level of the coupler. Their phase is a random value that cannot be determined experimentally. They are defined through their average quadratic properties:

$$\left\langle |(u^+)|^2 \right\rangle = \left\langle |(u^-)|^2 \right\rangle, \tag{6a}$$

$$\langle (u^+)(u^-)^* \rangle \approx 0. \tag{6b}$$

They can be related to the "intrinsic" spectral intensity $I_U(\omega)$ generated in the active zone, that is the intensity that would be coupled into the mode after a single loop [22]:

$$I_U(\omega) = \frac{\epsilon_0}{2} c\, n_{\text{eff}} \left\langle |(u^\pm)|^2 \right\rangle, \tag{7a}$$

$$= \beta_{\text{sp}}\,\hbar\omega\, r_{\text{sp}}(\omega) \frac{\exp(g_R L_R) - 1}{g_R}, \tag{7b}$$

where n_{eff} is the effective index of the ring, $r_{\text{sp}}(\omega)$ the spectral rate of spontaneous emission per unit volume [in $s^{-1}.(\text{rad}/s)^{-1}.m^{-3}$] and β_{sp} the fraction of spontaneous emission that couples into the ring mode. Note that $I_U(\omega)$ is completely determined by the optical properties of the active zone. Besides, if we assume $g_R L_R \ll 1$ (a quite reasonable assumption in most practical cases), then I_U is simply proportional to the perimeter L_R of the active ring:

$$I_U(\omega) \approx \beta_{\text{sp}}\,\hbar\omega\, r_{\text{sp}}(\omega) L_R. \tag{8}$$

This value should not be confused with that of the actual field that accumulates inside the cavity. When the four-port system is compacted into a two-port network, the relationship between input and output waves at remaining ports 1 and 2 takes the following form:

$$b_1 = t_R a_2 + (u^-) k_c/D_R, \tag{9a}$$
$$b_2 = t_R a_1 + (u^+) k_c/D_R, \tag{9b}$$

which can also be written as an extended (3×3) scattering matrix relationship:

$$\begin{pmatrix} b_1 \\ b_2 \\ 1 \end{pmatrix} = \begin{pmatrix} 0 & t_R & (u^-) k_c/D_R \\ t_R & 0 & (u^+) k_c/D_R \\ 0 & 0 & 1 \end{pmatrix} \begin{pmatrix} a_1 \\ a_2 \\ 1 \end{pmatrix}. \tag{10}$$

The background output source terms $(u^{\pm}) k_c/D_R$ are the waves that come out of the ring even when no wave is going in $(a_1 = a_2 = 0)$. We would like to point out that they are simply expressed as the product of the relevant equivalent field by the outcoupling coefficient k_c, projected into the resonance of the ring (made manifest by the denominator D_R). In other words, whatever the intrinsic spectral behavior of spontaneous emission, emitted fields bear the spectral signature of the resonance. This was to be expected: as observed in its time by Kastler on a Fabry–Perot, the radiation emitted by active atoms placed inside a cavity has to be coupled into its transfer function [23]. A ring resonator should not be different.

From the point of view of the straight waveguide, the above is even best expressed in terms of extended (3×3) transfer matrix formalism [16–19,22]. The structure with the co- and contrapropagating fields is schematically depicted in Fig. 4. The main interest of this formulation is that extended transfer matrices retain their cascadability. This property will be taken advantage of in Section 4. Whatever the boundary conditions, extended transfer matrix $[R]$ of the active ring connects the co-and contrapropagating waves between both abscissas z_c^- and z_c^+:

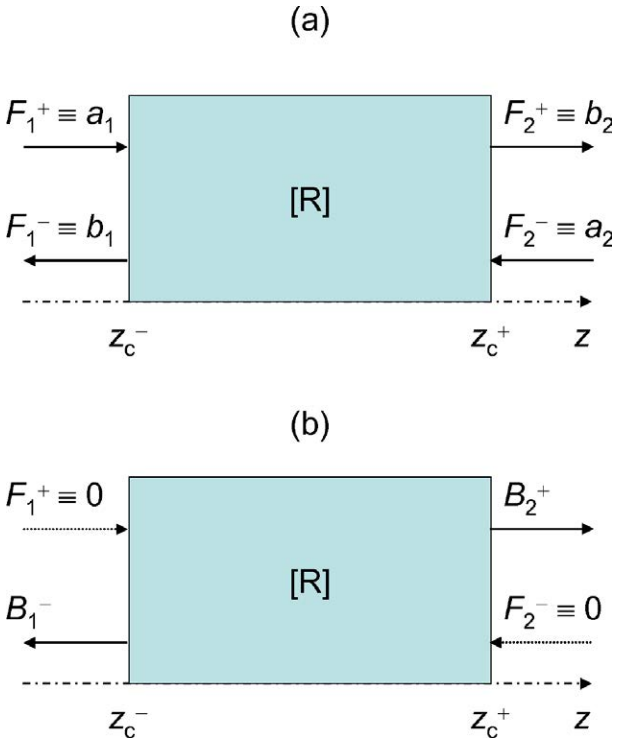

Fig. 4. Notations for extended Transfer Matrix Formalism connecting the co- and contrapropagating waves supported by the straight waveguide: (a) Input/output waves connected through ports (1) and (2) of the system ring + coupler; (b) background output waves (B_1^-, B_2^+) outcoupled from the system when no ingoing wave is present $(F_1^+ = F_2^- = 0)$.

$$\begin{pmatrix} F_1^+ \\ F_1^- \\ 1 \end{pmatrix} = \begin{pmatrix} R_{11} & 0 & R_{13} \\ 0 & R_{22} & R_{23} \\ 0 & 0 & 1 \end{pmatrix} \begin{pmatrix} F_2^+ \\ F_2^- \\ 1 \end{pmatrix}. \tag{11}$$

This gives exactly the same information as that provided by Eq. (10). We would like to emphasize that the first four coefficients $(R_{11}, R_{12}, R_{21}, R_{22})$ of transfer matrix $[R]$ are exactly the same as that of the usual (2×2) transfer matrix, according to the notations of Yariv and Yeh [24]. In the present case, the only non-vanishing coefficients (R_{11}, R_{22}) are related to the transfer function t_R of the ring resonator:

$$R_{11} = (1/t_R), \tag{12a}$$
$$R_{22} = t_R, \tag{12b}$$

whereas the source terms (R_{13}, R_{23}) in the third column are written as:

$$R_{13} = -(1/t_R)(u^+)(k_c/D_R), \tag{13a}$$
$$R_{23} = (u^-)(k_c/D_R). \tag{13b}$$

Not surprisingly, we recover the background fields (B_1^-, B_2^+) emitted at abscissas z_c and z_c^+ when no input field is present by applying the proper boundary conditions $(F_1^+ = F_2^- = 0)$:

$$B_1^- = R_{23} = (u^-)(k_c/D_R), \tag{14a}$$
$$B_2^+ = -R_{13}/R_{11} = (u^+)(k_c/D_R). \tag{14b}$$

As pointed out before, emitted fields appear filtered by the resonance of the cavity.

3. Generalized transfer function and threshold-crossing

3.1. Generalized transfer function

We have established the expression of the output fields; let us now concentrate on the internal fields $B^+(s)$ and $B^-(s)$ circulating inside the ring, where s is a curvilinear abscissa varying in the interval $[0, L_R]$, according to the notations of Fig. 5. Both $B^+(s)$ and $B^-(s)$ can be easily expressed in terms of the equivalent fields (u_P^+), (u_P^-), (u_Q^+) and (u_Q^-) generated by the active zones represented, respectively, by partial matrices $[P(s)]$ (of length s) and $[Q(s)]$ (of length $L_R - s$):

$$B^+(s) = \frac{1}{D_R}\left\{\left(u_P^+\right) + \left(u_Q^+\right) t_c' \exp\left(-i\beta_R s\right)\right\}, \tag{15a}$$
$$B^-(s) = \frac{1}{D_R}\left\{\left(u_Q^-\right) + \left(u_P^-\right) t_c' \exp\left(-i\beta_R (L_R - s)\right)\right\}. \tag{15b}$$

Note that each field B^+ or B^- takes the simple form of the "single-pass" linear combination of its relevant components, suitably projected into the resonance through the unmistakable denominator D_R. It should be noted that the equivalent fields (u^+) and (u^-), at both ends of the ring, are themselves expressed as weighted linear combinations of these partial (s-dependent) components:

$$(u^+) = \left(u_Q^+\right) + \left(u_P^+\right) \exp\left(-i\beta_R (L_R - s)\right), \tag{16a}$$
$$(u^-) = \left(u_P^-\right) + \left(u_Q^-\right) \exp\left(-i\beta_R s\right). \tag{16b}$$

Neglecting any standing wave pattern, as usual for a ring resonator, the local value of internal intensity is proportional to $\langle |B^+(s)|^2 + |B^-(s)|^2 \rangle$, where the brackets denote a time average. The spatially averaged spectral density of intensity $I_{AV}(\omega)$ of the intracavity field is readily obtained by integration along the curvilinear coordinate s, leading to

$$I_{AV}(\omega) = \frac{2 I_U(\omega)}{|D_R|^2}\left\{\left(\frac{1 - \eta^2 \tau_0^2}{g_R L_R}\right) - \left(\frac{1 - \tau_0^2 \eta^2 \gamma^2}{\gamma^2 - 1}\right)\right\}. \tag{17}$$

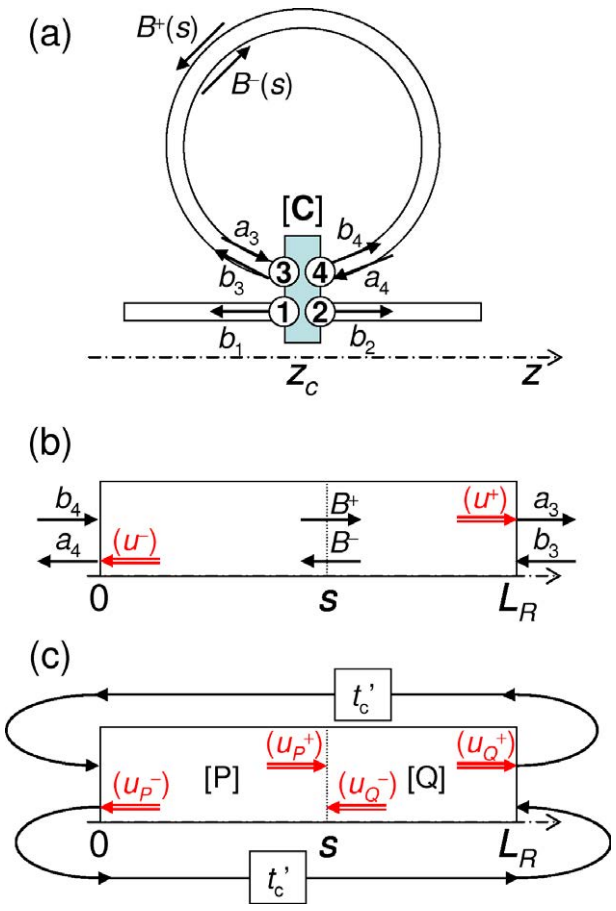

Fig. 5. (a)–(b) Notations for the internal fields: $B^+(s)$ and $B^-(s)$ propagate in both directions inside the ring, at curvilinear abscissa s in the interval $[0, L_R]$. (c) The ring itself can be decomposed into two active zones, respectively represented by partial matrices $[P(s)]$ and $[Q(s)]$, generating their own equivalent fields (u_P^+), (u_P^-), (u_Q^+) and (u_Q^-). Both ends are connected through the coupler.

This quantity constitutes the *generalized transfer function* (GTF) of the active ring resonator. Before proceeding further, we would like to comment upon its form. The GTF is proportional to the intrinsic intensity $2I_U(\omega)$ generated along the active zone (the factor 2 accounts for the two directions of propagation), corrected by a factor that is specific to the ring configuration, and projected into the resonance through the denominator $|D_R|^2$. Besides, it can be noted that in the vicinity of the threshold, the second term under brackets becomes vanishingly small as $1 - \tau_0^2 \eta^2 \gamma^2$ cancels out.

As a result, the GTF can be written as:

$$I_{AV}(\omega) = \frac{I_U(\omega) F(\omega)}{|D_R(\omega)|^2}, \tag{18}$$

where $F(\omega)$ is a slowly-varying function containing mostly opto-geometrical terms. Note that it takes the same general form as in a Fabry–Perot resonator, except for the detail of the function $F(\omega)$. The main result can be stated as follows: the spectral behavior of the internal field is completely determined by the denominator $D_R(\omega)$. This is especially important as far as gain saturation is concerned, as will become immediately apparent.

3.2. Threshold-crossing in an homogeneously broadened atomic medium

Up to now, we have not explicitly considered material dispersion; but since we work in the spectral domain, the chromatic dependence of the optical parameters is implicitly taken into account, all the same. For the sake of illustration, let us investigate the case of a ring where the gain comes from an homogeneously broadened atomic transition characterized by angular frequency ω_A and HWHM Γ_A, well described by its complex susceptibility $\chi = \chi' + i\chi''$ [25]:

$$\chi' = \chi_0 \left\{ \frac{X}{X^2 + 1 + Y} \right\} = X\, \chi'', \tag{19a}$$

$$\chi'' = \chi_0 \left\{ \frac{1}{X^2 + 1 + Y} \right\}, \tag{19b}$$

where X is the reduced detuning with respect to the center frequency:

$$X = \left(\frac{\omega - \omega_A}{\Gamma_A} \right), \tag{20}$$

Y is a dimensionless saturation parameter (proportional to the total saturating intensity, it will be taken as a measure of the normalized laser intensity), χ_0 a monotonously increasing function of the pumping level (we assume $\chi_0 \ll 1$). Real and imaginary parts are drawn in Fig. 6 for two values of the saturation parameter. It should be noted that the saturation affects not only the gain (through $\mathrm{Im}[\chi]$), but also the index (through $\mathrm{Re}[\chi]$), thus the precise value of the cavity resonance, that is the laser line, at angular frequency ω_L. We propose ourselves to derive the spectral and energetic properties of the laser across threshold, by using the GTF of the ring resonator. Since the medium is homogeneously broadened, the laser operates in a longitudinal single-mode regime, in the close vicinity of ω_L. The useful part of the GTF is reduced to a single Lorentzian lineshape, according to Eq. (4a). Apart from the specificity of the ring geometry, we follow closely an approach already exposed in [26].

Let us write the effective index and the modal gain of the ring as

$$n_R = n_H + \chi'/2, \tag{21a}$$

$$g_R = (\omega_A/c)\, \chi'', \tag{21b}$$

and χ_{th} the value reached by χ'' at the classical threshold. Refractive index n_H of the host medium is assumed constant over the gain spectral range, defining the "cold cavity" background ($n_R = n_H$ if $\chi' = 0$). The pumping level can be measured by reduced parameter $j_P = (\chi_0/\chi_{\mathrm{th}})$, which reaches unity at threshold.

For the sake of generality, let us work in reduced frequencies: $x = \omega L_R/c$, $x_A = \omega_A L_R/c$, $\xi_A = \Gamma_A L_R/c$, so that $X = (x - x_A)/\xi_A$. In the feeble-loss approximation, the GTF $I_{AV}(\omega)$ is written under its reduced form $y(x)$, well approximated by a Lorentzian:

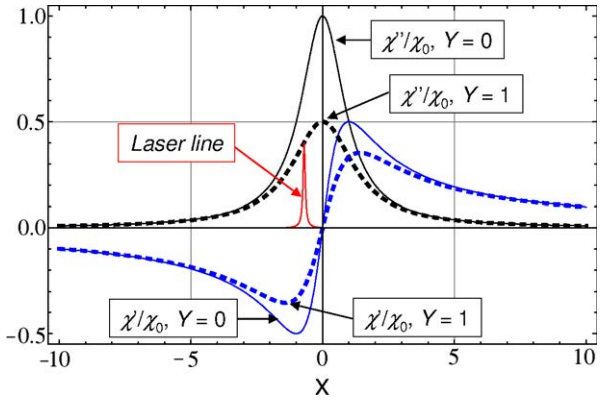

Fig. 6. Real and imaginary parts of normalized susceptibility in an homogeneously broadened atomic medium subject to population inversion, for two levels of the saturation parameter: $Y = 0$ (straight line), $Y = 1$ (dotted line). Imaginary part is responsible for the Lorentzian gain, real part for the S-like dispersion. The laser line is schematically plotted for comparison.

$$y(x) = y(x_L)\,\frac{\xi_L^2}{(x-x_L)^2+\xi_L^2}, \tag{22}$$

much sharper than the atomic line ($\xi_L \ll \xi_A$), as schematically shown in Fig. 6; by integrating over its whole spectral range, we obtain immediately:

$$Y = \int y(x)\,dx = y(x_L)\,\pi\,\xi_L. \tag{23}$$

The problem consists in determining simultaneously the laser frequency x_L, the total intensity Y and the linewidth ξ_L as a function of the only accessible experimental parameter: the pumping level j_P.

Susceptibility describes the material parameters; besides, optical intensity Y evolves according to

$$(dY/dt) = v_g\,(g_R - g_{\rm th})\;Y + S_Y, \tag{24}$$

where v_g is the group velocity and S_Y a source term. The spectral rate of spontaneous emission, assumed to be proportional to χ'', exhibits the same kind of Lorentzian behavior. Of course, it is also subject to saturation. In steady-state regime, we obtain therefore:

$$Y = \frac{S_Y/v_g}{(g_{\rm th}-g_R)} = \frac{\kappa\,\chi''}{(\chi_{\rm th}-\chi'')}, \tag{25}$$

where κ is a constant that characterizes the coupling of spontaneous emission into the mode, and χ'' should be evaluated at (as yet unknown) laser frequency x_L, which depends on a phase condition:

$$n(x_L)\,x_L = 2q\,\pi \tag{26}$$

or (q is an integer)

$$x_L\left[n_H + X_L\,\frac{\chi''}{2}\right] = 2q\,\pi. \tag{27}$$

Introducing parameters $(x_L/\xi_A) \approx (x_A/\xi_A) = (\omega_A/\Gamma_A) = Q_A$ (quality factor of the atomic transition), X_0 (resonance of the "cold" cavity) and $B = Q_A\,\xi_{\rm th}/(2\,n_H)$, one can establish two relationships between the laser frequency (X_L) and its power (Y) as a function of pumping (j_P), depending on three parameters only (κ, X_0, B):

$$X_L\left[1 + j_P\left(\frac{B}{X_L^2+1+Y}\right)\right] \approx X_0, \tag{28}$$

$$Y = \frac{\kappa\,j_P}{X_L^2+1+Y-j_P}. \tag{29}$$

Let us examine successively the case where the cavity is tuned or detuned with respect to the atomic transition. If both are tuned to the same frequency ($X_0 = 0$), the laser radiation coincides exactly with the line center ($\omega_L = \omega_0 = \omega_A$), and intensity Y is solution to a simple second-order equation:

$$Y^2 + Y\,(1-j_P) - \kappa j_P = 0. \tag{30}$$

Neglecting the source term ($\kappa = 0$), we recover exactly the limiting cases for a classical laser behavior: below threshold, $j_P < 1, Y = 0$; above threshold, $j_P > 1, Y = j_P - 1$. Actually, the transition across threshold is *continuous*, as illustrated in Fig. 7 for several values of κ.

If the cavity is detuned with respect to the atomic transition ($X_0 \neq 0$), intensity Y is the only physical solution to a fourth-order equation:

$$0 = \Big[Y^2 + Y\,(1-j_P) - \kappa j_P\Big]\,[Y\,(1+B)+\kappa]^2 + Y\,(Y+\kappa)^2\,X_0^2. \tag{31}$$

As far as frequency is concerned, X_L and X_0 share the same sign, with $|X_L| < |X_0|$. The laser line lies somewhere between the "cold cavity" resonance and the atomic transition:

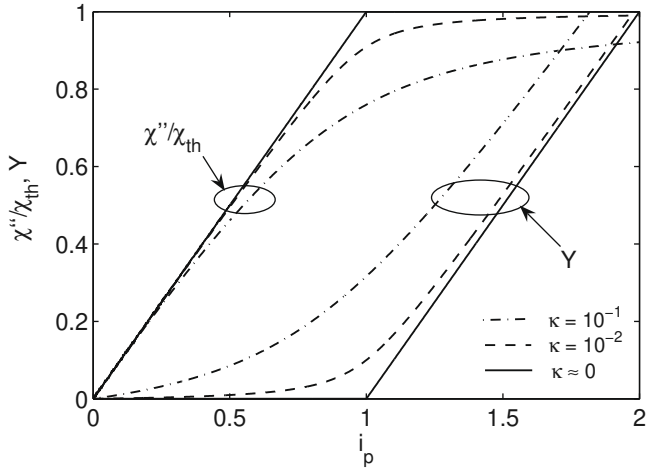

Fig. 7. Threshold-crossing in a microring resonator with an homogeneously broadened atomic transition, as a function of normalized pumping level j_P. Normalized gain $G = (\chi''/\chi_{\rm th})$ and photonic intensity Y, for $\kappa = 0, 10^{-1}, 10^{-2}$.

$$0 < \frac{X_L}{X_0} = \frac{\kappa + Y}{\kappa + Y\,(1+B)} < 1. \tag{32}$$

This is the well-known phenomenon of frequency-pulling, but we would like to point out that our approach enables one to follow continuously the emission frequency as a function of the pumping level: (X_L/X_0) evolves from 1 at $Y = 0$ to $1/(1+B)$ for $Y \gg \kappa$.

Besides, reduced linewidth (as compared to that at transparency), as shown in Fig. 8, is given by

$$\frac{\xi_L}{\xi_{\rm tr}} = \frac{\kappa}{(\kappa+Y)}. \tag{33}$$

It should be noted that in a strong enough laser regime ($Y \gg \kappa$), the product ($Y\,\xi_L$) tends toward a constant, according to the classical Schawlow–Townes formula:

This detailed example illustrates the high potential of the GTF formalism, as applied to threshold-crossing in single-mode microring geometries. In a semiconductor, a similar approach can be followed. As far as the optical properties of the active material are concerned, two levels of approximation can be considered [19].

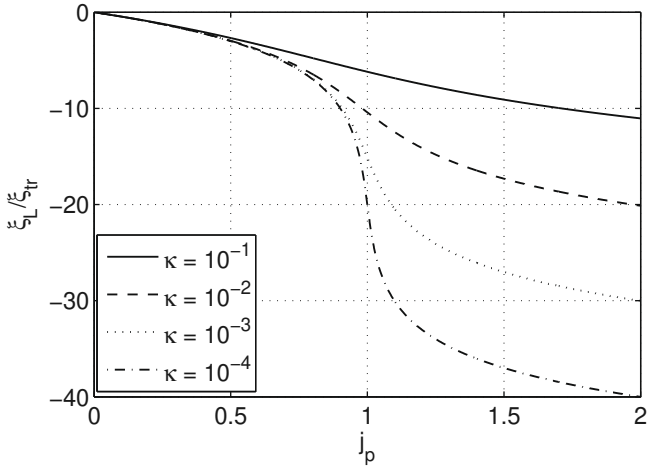

Fig. 8. Threshold-crossing in a microring resonator with an homogeneously broadened atomic transition, as a function of normalized pumping level j_P. Reduced linewidth $W = (\xi_L/\xi_{\rm tr})$ (with respect to transparency value $\xi_{\rm tr}$), expressed in dB, for $\kappa = 10^{-1}, 10^{-2}, 10^{-3}$ and 10^{-4}; note the high gain of coherence that goes with the passage across threshold.

At the simplest level, the effective index, the modal gain and the spectral rate of spontaneous emission are supposed to be uniquely determined by the carrier density N, assumed uniformly saturated along the active zone. Within the framework of the rate equation formalism, the steady-state value of N results from a balance between pumping and recombination processes. At a second level, they can also depend on the total density of optical power, sometimes described through a single photonic parameter P ("photonic density") [27].

The principles being thoroughly exposed, we explore in the last section some further implications of the formalism.

4. Possible extensions, perspectives and conclusions

4.1. Extended cavity schemes

As an illustration of the potential of extended (3×3) transfer matrix formalism, let us have a look at the extended microring cavity as schematically depicted in Fig. 9, where the left arm of the straight waveguide is terminated by a passive reflector, represented by its own transfer matrix $[A]$.

Between abscissas z_0 (before the first reflector) and z_S (just after the ring), matrix $[M]$ reads:

$$[M] = [A] \begin{pmatrix} e^{+i\beta_S d} & 0 & 0 \\ 0 & e^{-i\beta_S d} & 0 \end{pmatrix} [R], \tag{34}$$

where $[R]$ is given by Eq. (11) and

$$[A] = \begin{pmatrix} A_{11} & A_{12} & 0 \\ A_{21} & A_{22} & 0 \\ 0 & 0 & 1 \end{pmatrix}. \tag{35}$$

Since part of the field is reflected back toward the ring on reflector $[A]$, it seems only natural to expect a marked effect on the laser threshold, the more pronounced as the reflection is higher. However, intuitions can be deceptive, sometimes: since $M_{11} = A_{11} R_{11} \exp(+i\beta_S d)$, the classical threshold condition $M_{11} = 0$ is strictly equivalent to $R_{11} = 0$. Funnily enough, the external mirror has no effect whatsoever on the modal cartography (spectral position of the oscillation modes and associated threshold gain). Of course, for symmetry reasons, it would be the same if the reflector were located on the right arm of the straight waveguide.

The effect of the reflector is to be looked for elsewhere: background fields (B_0^-, B_S^+) emitted from the cavity at abscissas z_0 and z_S when no input field is present $(F_0^+ = F_S^- = 0)$ have become:

$$B_S^+ = -M_{13}/M_{11}, \tag{36a}$$

$$B_0^- = (M_{23} M_{11} - M_{13} M_{21})/M_{11}. \tag{36b}$$

Emitted fields appear filtered into the transfer function $t = 1/M_{11}$ of the whole cavity. So is the internal field, as expressed by the GTF. Source terms are also affected:

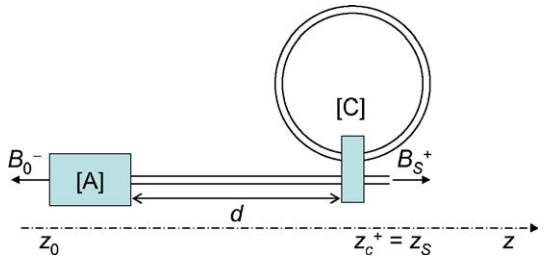

Fig. 9. Extended microring cavity, with a reflector on the left arm of the straight waveguide, represented by its transfer matrix $[A]$. The overall extended transfer matrix $[M]$ of the whole system is simply given by a matrix product.

$$M_{13} = R_{13} A_{11} \exp(+i\beta_S d) + R_{23} A_{12} \exp(-i\beta_S d), \tag{37a}$$

$$M_{23} = R_{13} A_{21} \exp(+i\beta_S d) + R_{23} A_{22} \exp(-i\beta_S d). \tag{37b}$$

Extended (3×3) transfer matrix function (TMF) is thus an elegant as well as powerful modeling tool, perfectly suited for investigating cascaded elements, such as chains of active ring resonators connected to the same straight waveguide.

Besides, since transfer matrices do not depend upon the boundary conditions (except insofar as gain saturation is concerned), it provides us with a simple way of dealing with optical seeding, where one (or several) external optical signal(s) is (are) injected through one (or more) input ports. The GTF exhibits a composite expression, with internal as well as external source terms, all affected by specific weighting coefficients, but all projected into the "classical" resonance through the common denominator D_R.

4.2. Active ring connected to two passive straight waveguides

It so happens that a microring resonator is sometimes simultaneously coupled to two parallel straight waveguides (Fig. 10). In the non-linear regime, care should be taken that the two halves of the ring do not necessarily experience the same intensity, so that differential saturation may break the symmetry. That is the reason why the equivalent fields are defined independently, with each section between two adjacent ports assumed uniformly saturated. Subscript "g" is relative to the left-hand half ("g" stands for "gauche" in French), subscript "d" to the right-hand half ("droit" in French). Applying the same approach as exposed in Section 2, we derive eventually the extended scattering matrix of the reduced four-port system:

$$\begin{pmatrix} b_1 \\ b_2 \\ b_3 \\ b_4 \\ 1 \end{pmatrix} = \begin{pmatrix} 0 & S_{12} & S_{13} & 0 & S_{15} \\ S_{21} & 0 & 0 & S_{24} & S_{25} \\ S_{31} & 0 & 0 & S_{34} & S_{35} \\ 0 & S_{42} & S_{43} & 0 & S_{45} \\ 0 & 0 & 0 & 0 & 1 \end{pmatrix} \begin{pmatrix} a_1 \\ a_2 \\ a_3 \\ a_4 \\ 1 \end{pmatrix} \tag{38}$$

with

$$S_{12} = \frac{t_1 - \eta_1^2 t_2' \gamma_g \exp\left(-i\varphi_g\right) \gamma_d \exp(-i\varphi_d)}{D_R}, \tag{39a}$$

$$S_{13} = \frac{k_1 k_2 \gamma_d \exp(-i\varphi_d)}{D_R}, \tag{39b}$$

$$S_{15} = \left(u_d^-\right) \frac{k_1}{D_R} + \left(u_g^-\right) \frac{k_1 t_2' \gamma_d \exp(-i\varphi_d)}{D_R}. \tag{39c}$$

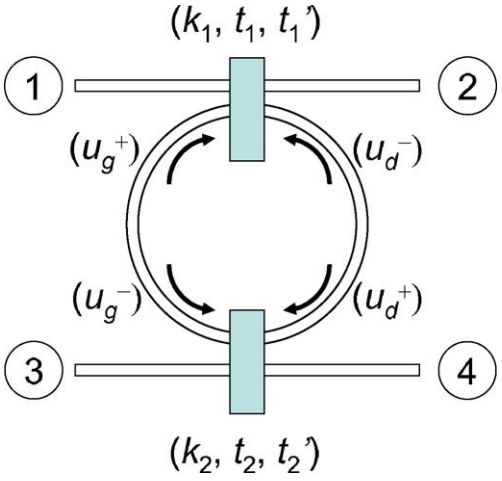

Fig. 10. Active microring coupled to two parallel (not necessarily identical) passive straight waveguides. Parameters of the upper and lower couplers are (k_1, t_1, t_1') and (k_2, t_2, t_2') respectively. The whole system is seen as a multiple-port network.

The denominator is given by

$$D_R = 1 - t'_1 t'_2 \gamma_g \exp\left(-i\varphi_g\right) \gamma_d \exp\left(-i\varphi_d\right) \tag{40a}$$

$$= 1 - t'_1 t'_2 \gamma \exp\left(-i\varphi\right), \tag{40b}$$

where $\varphi = \varphi_g + \varphi_d$ is the total phase change and $\gamma = \gamma_g \gamma_d$ the total amplitude change. The derivation of the other coefficients follows the same line and is therefore left to the reader's appreciation. So is the extended (5×5) transfer matrix, enabling one to cascade successive active rings and derive the overall GTF. We would like to point out, once again, that the form taken by each *S*-parameter (classical or extended) appears to the trained eye as highly predictable: the numerator indicates the direct single-path from one port (or from one intrinsic contribution) to the output port under consideration; then the expression is simply corrected through the denominator that indicates the resonant behavior. Note that the numerator of S_{12}, slightly more complex than that of S_{13}, expresses the interference between the direct path and the loop path.

4.3. Conclusions and perspectives

The generalized transfer function of an active single-mode microring resonator (representing the spectral density of intracavity field intensity) has been derived in the frame of extended Scattering and/or Transfer Matrix formulations. Spontaneous emission, looked upon as the driving source of the radiation, is described in a semi-classical way in the spectral domain. The internal and emitted fields are filtered into the resonance modes of the whole structure. The generalized transfer function contains all essential mechanisms at work in a laser oscillator: gain, losses and sources. The active zone is saturated through amplified spontaneous emission, integrated over its whole spectral range. Continuously valid across threshold, the method enables one to derive in a simple way the main steady-state properties of the laser oscillation, with the pumping rate as the only external parameter. In this approach, the optical properties of the active medium (the gain, the source and the refractive index) are supposed to be uniquely determined by the steady-state value of the material parameters, assumed uniform along the active zone.

As far as thermal effects are concerned, they would modify not only the optical properties, but also the very geometry of the resonator, because of thermal expansion [28]. If we can assume that (i) temperature *T* is reasonably homogeneous at the scale of the whole active waveguide; (ii) its variation is a known function of the pumping level; then the same approach can nevertheless be applied, since the spectral properties of the resonance mode remain uniquely determined by the given set of parameters.

Along with the GTF approach, extended Scattering and/or transfer matrix formalisms constitute an elegant and powerful modelling tool for investigating a lot of configurations involving active single-mode microring resonators. The above list of possible extensions is far from exhaustive: to cite but a few others, dual-wavelength lasing in whispering gallery mode rare-earth-doped microspheres, or second harmonic generation in semiconductor microdisks are currently under investigation.

Acknowledgements

The authors would like to thank Prof. G.M. Stéphan, former Head of Optronics Laboratory at ENSSAT (Lannion) and Dr. Y. Dumeige from ENSSAT–FOTON, for stimulating discussions. Y.G. Boucher would like to express its gratitude to the French Centre National de la Recherche Scientifique (CNRS) for having made materially possible a one-year leave entirely dedicated to scientific research (so-called Délégation).

References

[1] R.K. Chang, A.J. Campillo, Optical Processes in Microcavities, World Scientific, Singapore, 1996.
[2] K.J. Vahala, Optical Microcavities, World Scientific, Singapore, 2004.
[3] V.B. Braginsky, M.L. Gorodetsky, V.S. Ilchenko, Phys. Lett. A 137 (1989) 393.
[4] L. Collot, V. Lefèvre-Seguin, M. Brune, J.-M. Raimond, S. Haroche, Europhys. Lett. 23 (1993) 327.
[5] B.E. Little, S.T. Chu, H.A. Haus, J. Foresi, J.P. Laine, J. Lightwave Technol. 15 (1997) 998.
[6] J.E. Heebner, P. Chak, S. Pereira, J.E. Sipe, R.W. Boyd, J. Opt. Soc. Am. B 21 (2004) 1818.
[7] D.G. Rabus, Integrated Ring Resonators, Springer-Verlag, Berlin, 2007.
[8] T. Baer, Opt. Lett. 12 (1987) 392.
[9] V. Sandoghdar, F. Treussart, J. Hare, V. Lefèvre-Seguin, J.-M. Raimond, S. Haroche, Phys. Rev. A 54 (1996) 1777.
[10] F. Lissillour, P. Féron, N. Dubreuil, P. Dupriez, M. Poulain, G.M. Stéphan, Electron. Lett. 36 (2000) 1382.
[11] S.L. McCall, A.F.J. Levi, R.E. Slusher, S.J. Pearton, R.A. Logan, Appl. Phys. Lett. 60 (1992) 289.
[12] M. Fujita, T. Baba, Appl. Phys. Lett. 80 (2002) 2051.
[13] M. Sorel, G. Giuliani, A. Scirè, R. Miglierina, S. Donati, P.J.R. Laybourn, IEEE J. Quantum Electron. 39 (10) (2003) 1187.
[14] G.M. Stéphan, Phys. Rev. A 55 (2) (1997) 1371.
[15] G.M. Stéphan, Quantum Semiclass. Opt. 10 (1998) 1.
[16] J.-P. Weber, S. Wang, IEEE J. Quantum Electron. 27 (10) (1991) 2256.
[17] J.-P. Weber, IEEE J. Quantum Electron. 29 (1) (1993) 296.
[18] Y.G. Boucher, Res. Signpost: Recent Res. Devel. Opt. (3) (2003) 177.
[19] Y.G. Boucher, S. Blin, P. Besnard, G.M. Stéphan, Proc. SPIE 5452 (2004) 654.
[20] A. Yariv, Electron. Lett. 36 (2000) 321.
[21] H.K. Choi, K.L. Chen, S. Wang, IEEE J. Quantum Electron. QE-20 (4) (1984) 385.
[22] Y.G. Boucher, J. Eur. Opt. Soc. Rap. Public. 1 (2006) 06027.
[23] A. Kastler, Appl. Opt. 1 (1962) 17.
[24] A. Yariv, P. Yeh, Optical Waves in Crystals, Wiley, New York, 1984.
[25] A.E. Siegman, Lasers, University Science Books, Mill Valley, 1986.
[26] Y.G. Boucher, J. Phys. IV France 135 (2006) 103.
[27] E. Rosencher, B. Vinter, Optoelectronics, Cambridge University Press, 2002.
[28] Z.P. Cai, H.Y. Xu, G.M. Stéphan, P. Féron, M. Mortier, Opt. Commun. 229 (2004) 311.